

# We are IntechOpen, the world's leading publisher of Open Access books Built by scientists, for scientists

6,900

Open access books available

186,000

International authors and editors

200M

Downloads

Our authors are among the

154

Countries delivered to

TOP 1%

most cited scientists

12.2%

Contributors from top 500 universities



WEB OF SCIENCE™

Selection of our books indexed in the Book Citation Index  
in Web of Science™ Core Collection (BKCI)

Interested in publishing with us?  
Contact [book.department@intechopen.com](mailto:book.department@intechopen.com)

Numbers displayed above are based on latest data collected.  
For more information visit [www.intechopen.com](http://www.intechopen.com)



---

# High Resolution Radargrammetry – 3D Terrain Modeling

---

Paola Capaldo, Francesca Fratarcangeli,  
Andrea Nascetti, Francesca Pieralice,  
Martina Porfiri and Mattia Crespi

Additional information is available at the end of the chapter

<http://dx.doi.org/10.5772/57483>

---

## 1. Introduction

Radargrammetry is a methodology to extract 3D geometric information from Synthetic Aperture Radar (SAR) imagery. Similarly to photogrammetry, radargrammetry forms a stereo model. The continuous observations of the Earth's surface by satellite SAR sensors with short revisit times enable a near real-time 3D Earth surface mapping through Digital Surface Models (DSMs). Such products have a large relevance in territorial applications, such as topographic mapping, spatial and temporal change detection, morphological feature extraction, geographic data management, and visualization. SAR satellite systems provide information independently from logistic constraints on the ground (as for airborne data collection), illumination (daylight) and weather (clouds) conditions. Starting from the SAR data, two different approaches can be considered: the phase-based interferometric techniques and the intensity-based radargrammetric ones. Being aware that radar interferometry may suffer for lack of coherence, the two methods are thus complementary to achieve the most accurate and complete results. Radargrammetry was first used in the 1950s and then less and less exploited. The low resolution in amplitude supplied by the first spaceborne radar sensors (around 20 m) didn't raise more attractiveness. From 2007, the availability of very high resolution SAR data (up to 1 m Ground Sample Distance (GSD)) from COSMO-SkyMed, TerraSAR-X and RADARSAT-2 data allowed new developments. For instance Raggam et al. [1] studied the potentialities of TerraSAR-X, while Toutin [2] studied the RADARSAT-2 ones.

In this chapter, we focus on the radargrammetric approach and propose a complete procedure for generating DSMs starting from zero Doppler focused high resolution SAR imagery. A tool for radargrammetric processing of high resolution satellite SAR stereo pairs was implemented in the scientific software SISAR (Software per le Immagini Satellitari ad Alta Risoluzione), developed at the Geodesy and Geomatic Division of the University of Rome "La Sapienza" [3].

Two steps are necessary for radargrammetric DSM extraction: the image orientation and the image matching (automatic detection of homologous points).

As regards the orientation model (discussed in paragraph 2), it was established, starting from the rigorous model proposed in Leberl [4], in paying attention to the orbital model represented with Lagrange polynomials to exploit the potential of the novel high resolution (both in azimuth and in range). The Rational Polynomial Functions (RPFs) model based on Rational Polynomial Coefficients (RPCs) was also considered. The RPCs can be a useful tool in place of the rigorous model in the processes of image orthorectification/geocoding or as the DSMs generation. This generalized method is standard and unique for all sensors. The performances of the RPFs model using the RPCs can reach the level of the rigorous model. A terrain independent procedure to generate RPCs starting from radargrammetric model was defined. The possibility to generate RPCs sounds of particular interest since, at present, most part of SAR imagery is not supplied with RPCs (only in RADARSAT-2 metadata the RPCs are available), although the RPFs model is available in several commercial software.

The matching process (discussed in paragraph 3) is the automatic identification of pixels representing the same object in two or more images. If corresponding pixels are recognized, then a simple geometric intersection is needed to compute the position of their corresponding object in space. The development of a fully automatic, precise and reliable image matching method that adapts to different images and scene contents is a challenging problem. Dissimilarities between SAR images due to occlusion, illumination differences, radiometric differences and speckle noise must be taken into account. Many different image matching approaches have been developed in recent years, both within the photogrammetry and computer vision research fields. In all matching algorithms, there are two fundamental aspects that must be taken into account: the definition of a primitive model, and consequently of an identification criterion, and the choice of a strategy for the search of corresponding pixel (also named homologous points in photogrammetry) on a couple (or more) images.

An additional problem for SAR imagery is the speckle, which significantly impedes the image matching. Speckle filtering strategies were investigated, to be applied before matching. The images geometric configuration also impacts image matching. The optimum stereo imagery configuration for the radargrammetric application is when the target is observed in opposite-side view. However it causes large geometric and radiometric disparities, hindering the image matching. A good compromise is in the use of a same-side configuration stereo pair with a convenient base to height ratio, to increase the efficiency in the correlation image process [5].

As regards image matching, an original strategy was defined and implemented. The algorithm is based on an hierarchical solution with a geometrical constrain and the correspondences are looked using an area based matching criterion and analysing the Signal to Noise Ratio (SNR).

To demonstrate the radargrammetric mapping potential of high resolution SAR satellite imagery, several tests were carried out using data acquired in SpotLight mode and coming from COSMO-SkyMed, TerraSAR-X. They are presented in paragraph 4. Finally, conclusion and ideas for future work are outlined in paragraph 5.

## 2. Stereo SAR geometry

Radargrammetry is based on stereogrammetry, a classic method for relief reconstruction using optical remote sensing images. Stereo viewing reproduces the natural process of stereovision. Figure 1 represents the radargrammetric SAR geometry,  $S_1, S_2$  are the satellites,  $B_x, B_z$  the horizontal and vertical baseline respectively;  $R_1, R_2$  the distances between the sensors and the ground target  $P$ . Target  $P$  is seen as  $P_1$  and  $P_2$  in both SAR images from  $S_1$  and  $S_2$ .

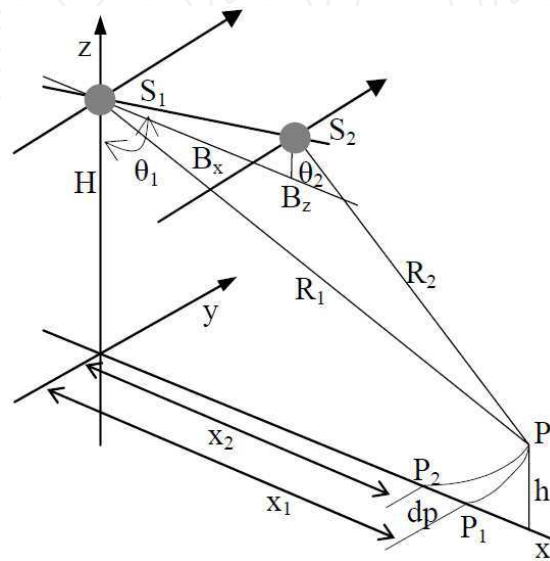


**Figure 1.** The different observation positions and geometry for radargrammetry

The differences between images is measured to establish a disparity map. It is used to compute the terrain elevation from the measured parallaxes between the two images [6].

In the 1960s, stereoscopic methods were applied to radar images to derive ground elevation leading to the development of radargrammetry [7]. It was shown that some specific SAR stereo configurations would produce the same elevation parallaxes as those produced by aerial photos.

To orientate the SAR imagery, several models were developed, based on classical radar [4] equations and physical constrains [8].

### 2.1. SAR imagery rigorous orientation model

#### 2.1.1. Observation equation

The radargrammetric rigorous model implemented in SISAR is based on the equation of radar target acquisition and zero Doppler focalization. Radargrammetry performs a 3D reconstruction based on the determination of the sensor-object stereo model, in which the position of each point on the object is computed as the intersection of two radar rays coming from different positions and therefore with two different look angles (Figure 2).

These radar rays are modeled as two segments centered along two different satellite orbits. The intersection generating each object point is one of the two possible intersections between two circumferences centered in the two different positions and laying into two planes

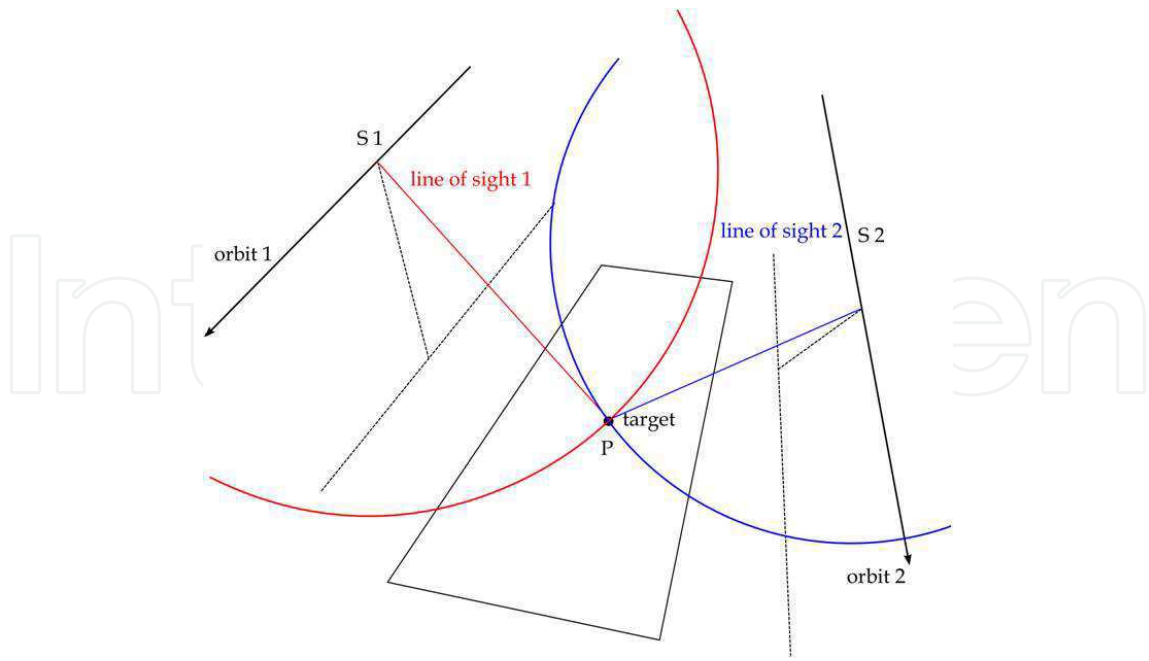


**Figure 2.** SAR acquisition system in zero Doppler geometry

orthogonal to the two satellite orbits whose radii are equal to the segment measured lengths [9]. The first equation of (1) is the slant range constrain. The second equation of (1) represents the orthogonality condition between each radar ray heading and the flying direction of the satellite. The couple of equations in a ECEF (Earth Centered Earth Fixed) system (for example WGS84) reads:

$$\begin{cases} \sqrt{(X_P - X_S)^2 + (Y_P - Y_S)^2 + (Z_P - Z_S)^2} - (D_s + \Delta r \cdot I) = 0 \\ u_{S_x} \cdot (X_P - X_S) + u_{S_y} \cdot (Y_P - Y_S) + u_{S_z} \cdot (Z_P - Z_S) = 0 \end{cases} \quad (1)$$

where:

- $X_P, Y_P, Z_P$  are the coordinates of the generic ground point P in the ECEF coordinate system
- $X_S, Y_S, Z_S$  are the coordinates of the satellite in the ECEF coordinate system
- $u_{X_S}, u_{Y_S}, u_{Z_S}$  are the Cartesian components of the satellite velocity in the ECEF coordinate system
- $D_s$  is the so-called "near range"
- $\Delta r$  is the slant range resolution or column spacing
- $I$  is the column position of point P on the image

The acquisition time of each line  $t$  can be related to line number  $J$  through a linear function (2), since the satellite angular velocity can be considered constant along the short orbital arc related to the image acquisition:



$$p_{k+1}(x) = p_k(x) + f[x_0, x_1, \dots, x_{k+1}] \cdot (x - x_0) \cdot (x - x_1) \cdot (x - x_{k+1}) \quad (6)$$

where  $p_k(x)$  is the interpolation polynomial of degree  $k$  on ties  $x_0, x_1, \dots, x_k$ . The ties  $x_0, x_1, \dots, x_k$  are the state vector time and the  $f(x_0), f(x_1), \dots, f(x_k)$  represent either the position state vector to define satellite flight path or the velocity state vector to calculate the satellite velocity [10]. Lagrange polynomial interpolation is enough accurate to model the short orbital segment and its well-known problems at the edges do not affect the modeling since the images are acquired in the central part of the orbital segment. Additionally, using a standard divide and conquer algorithm, it is possible to find in a rapid and accurate way the epoch when satellite orbit is perpendicular to the line of sight between the sensor and the generic ground point.

### 2.1.3. Metadata Tie Points: a tool for orientation model check

TerraSAR-X and RADARSAT-2 products have in the metadata a number of Tie Points (TPs) distributed on a regular grid. These points were calculated directly by the image providers, using the intrinsic radar geometry acquisition model. These points have image and ground coordinates, so the object coordinates of each point were used to determinate the image coordinates with the model implemented in SISAR. The image coordinates residuals shown that the defined and implemented model is quite compliant with the intrinsic SAR acquisition geometry at sub-pixel level (Table 1).

SAR image	BIAS TPs		ST. DEV. TPs		RMSE TPs	
	I	J	I	J	I	J
Hannover 05/12/2007	0.25	0.32	0.28	0.26	0.38	0.41
Hannover 10/12/2007	0.31	0.39	0.29	0.29	0.43	0.49
Hannover 29/12/2007	0.47	0.40	0.30	0.28	0.55	0.48
Trento 19/01/2011	0.30	0.41	0.30	0.31	0.42	0.52
Trento 14/01/2011	-0.50	0.27	0.30	0.58	0.58	0.39

**Table 1.** Accuracy result on metadata Tie Points (example for TerraSAR-X) [pix]

### 2.1.4. Impact of GCPs errors on stereo orientation accuracy

The Ground Control Points (GCPs) selection on radar imagery is much more difficult than on the optical one, and it is possible to misregister their positions (Figure 3). To evaluate the impact of GCPs collimation errors on the accuracy of stereo orientation, a Monte Carlo simulation was used. Starting from a no errors configuration, a Gaussian error was applied, with 1 to 6 pixel standard deviation (common values are around 1 to 4 pixels) to GCPs image coordinates, to simulate collimation errors of different magnitude. The stereo pair was oriented using a different number of GCPs (3, 6, 9); for each orientation (3, 6, 9 GCPs) 100 orientations affected by random errors were computed, at last the orientation accuracy was evaluated computing the RMSE calculated on Check Points (CPs) ground coordinates residuals. The results shown that the RMSE error due to the collimation on radar image is at level of 1 - 2 m in horizontal coordinates and 1 m in vertical ones even if the number of GCPs increases, the accuracy does not significantly.

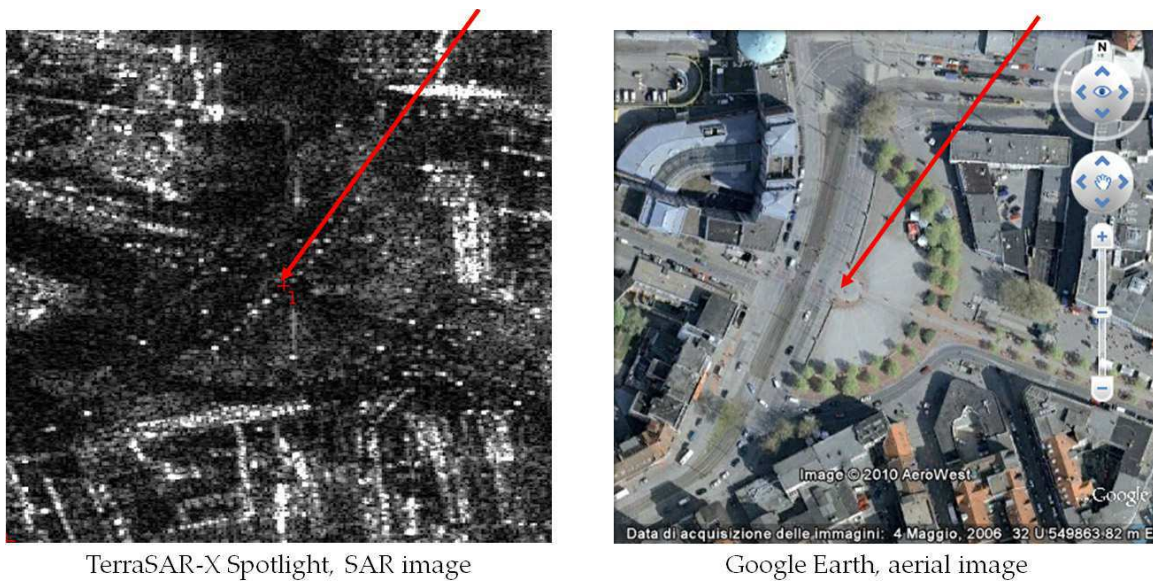


**Figure 3.** Visual comparison between radar and optical collimation of the same detail

Therefore, the collimation errors have a great impact on the finally accuracy of stereo orientation, so that the possibility to orientate the images directly, on the bases of the refined orbital model and the metadata parameters represent an opportunity to remove the effect of collimation errors and increase the orientation accuracy.

The accuracy results of orientation model performed without GCPs are closer to the results computed with a model based on GCPs refinement [11].

## 2.2. SAR imagery orientation with RPCs re-parametrization

The Rational Polynomial Functions model is a method to orientate optical satellite imagery. Currently all optical images supply, together imagery, the RPCs file generated starting from the own rigorous model. On the contrary, regarding SAR images only RADARSAT-2 have a RPCs file whereas COSMO-SkyMed and TerraSAR-X images are devoid. On the other hand the use of the RPFs model is common in several commercial software for two reasons: the implementation of the RPFs model is standard, unique for all sensors, and much simpler that the one of a rigorous model, which has to be customized for each sensor, and the performance of the RPFs model can be at the level of the ones from rigorous models. The RPCs generation on the basis of rigorous orientation sensor models is an important tool.

RPFs model relates the object point coordinates (latitude  $\phi$ , longitude  $\lambda$  and height  $h$ ) to the pixel coordinates ( $I, J$ ) in the form of ratios of polynomial expressions (7) whose coefficients (RPCs) are often supplied together with imagery:

$$I = \frac{P_1(\phi, \lambda, h)}{P_2(\phi, \lambda, h)} \quad J = \frac{P_3(\phi, \lambda, h)}{P_4(\phi, \lambda, h)} \quad (7)$$

The number of the RPCs depends on the polynomial order (usually limited to the third one), so that each of them takes the generic form (8):

$$P_n = \sum_{i=0}^{m_1} \sum_{j=0}^{m_2} \sum_{k=0}^{m_3} t_{ijk} \cdot \phi^i \cdot \lambda^j \cdot h^k \quad (8)$$

with  $0 \leq m_1 \leq 3$ ;  $0 \leq m_2 \leq 3$ ;  $0 \leq m_3 \leq 3$  and  $m_1 + m_2 + m_3 \leq 3$  where  $t_{ijk}$  are the RPCs. In case of third order polynomials, the maximum number of coefficients is 80 (20 for each polynomial); actually, it is reduced to 78, since the two equations (7) can be divided for the zero order term of their denominators. The image and ground coordinates in equation are usually normalized to (-1, +1) range to improve the numerical accuracy, using the formula (9):

$$T_n = \frac{T - T_{offset}}{T_{scale}} \quad (9)$$

where  $T_n$  are the normalized coordinates;  $T_{offset}$ ,  $T_{scale}$  are the normalization parameters available in the metadata file; and  $T$  is the generic original ground or image coordinate ( $T = I, J; \phi, \lambda, h$ ).

In principle, RPCs can be generated by a terrain-dependent scenario without using the physical sensor model or by a terrain independent scenario.

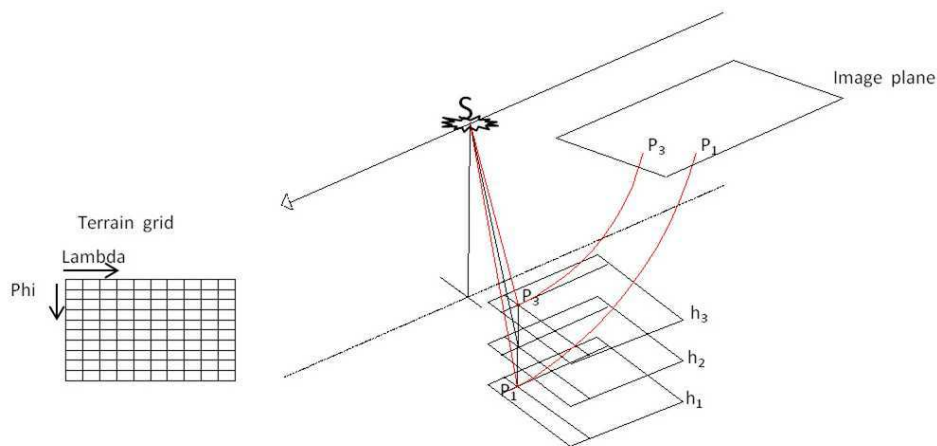


**Figure 4.** RPCs-terrain independent approach generation

Nevertheless, the first approach is not recommended for two relevant reasons. At first, it is likely to cause large deformations in areas far from the GCPs and it is very weak and vulnerable in presence of outliers. Further, it is not convenient, since the number of required GCPs could be very high. For example, at least 39 GCPs are necessary if RPCs up to the third order are looked for. On the contrary, following the second approach, RPCs can be generated using a known physical sensor model. This is the standard for some sensor managing companies, which supply through imagery metadata a re-parametrized form of the radargrammetric sensor model in term of RPCs, generated from their own secret physical sensor models [12, 13]. The developed and implemented procedure to generate

RPCs within SISAR includes three main steps: 1) at first the image is orientated through the already established radargrammetric rigorous orientation model; 2) further, 3D object grid with several layers slicing the entire terrain elevation range is generated; the horizontal coordinates of a point of the 3D object grid are calculated from the image corner coordinates with a regular posting, the corresponding  $(I, J)$  of the image grid are calculated using the computed orientation model; 3) finally, the RPCs are estimated in a least squares solution, having as input the coordinates of the 2D image grid points and of the 3D object grid points (Figure 4).

Investigations with optical imagery clearly underlined that many RPCs are highly correlated, so that the least squares problem is basically overparametrized. To avoid instability due to high correlations, leading to a pseudo-singular design matrix, usually a Tikhonov regularization is adopted, adding a damping factor to the diagonal of the normal matrix. On the contrary, in SISAR procedure, just the actually estimable RPCs are selected to avoid overparametrization (parsimony principle) [14, 15]). The Singular Value Decomposition (SVD) and QR decomposition are employed to evaluate the actual rank of the design matrix. To perform this selection, the remaining RPCs need to be constrained to zero [16]. Moreover, the statistical significance of each estimable RPC is checked by a Student T-test and the estimation process is repeated until only RPCs are selected.

### 3. SAR image matching

In general, the term image matching means automatic correspondence establishment, between primitives (homologous points) extracted from two or more digital images, depicting at least partly the same physical objects in space (Figure 5).

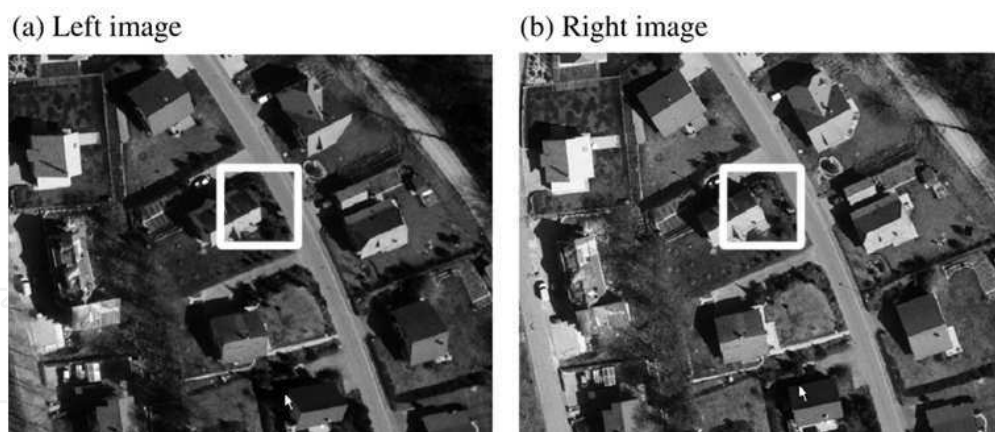


**Figure 5.** Example of homologous points in optical imagery

The fact that humans solve the correspondence problem, especially with optical imagery, so effortlessly should not lead us to think that this problem is trivial. On the contrary, humans exploit a remarkable amount of information to arrive at successfully declaring correspondence, including analysing context and neighbouring structures in the image and a prior information of the content of the scene. An image matching algorithm is a procedure able to solve the *correspondence problem* to obtain automatically a great number of homologous points [17].

### 3.1. An original matching strategy

The development of a fully automatic, accurate, and reliable image matching approach that adapts to different imagery (both optical and SAR) and scene contents is a challenging problem. Many different approaches to image matching have been developed within the photogrammetry and computer vision research fields [17–19]. Dissimilarities between SAR images due to occlusion, geometric distortions, radiometric differences and speckle noise must be taken into account leading to various approaches. Hereafter the basic features of an original matching strategy, presently under patenting by the University of Rome "La Sapienza", are outlined [20].

#### 3.1.1. Area selection and filtering

At the beginning of the image matching procedure, it is mandatory to select an area of interest and a coarse height range (approximate maximum and minimum terrain ellipsoidal heights), to reduce the object space and to remarkably decrease the processing time.

SAR imagery are affected by speckle hindering target recognition and correct matching (Figure 6). To reduce speckle, three different adaptive spatial filters (Lee, Kuan, GammaMap) have been considered for a preprocessing enhancement. Thanks to a number of tests, it was highlighted that these spatial filters significantly increase the number of points at the expense of vertical accuracy, since they mitigate the speckle but smooth the image features.

Starting from this experimental awareness, an original filtering procedure *dynamic filtering* has been developed, to maximize not only the number of points, but also their quality. Unlike the traditional preprocessing techniques, the image filtering is done directly during the matching procedure; the leading idea is to find out all possible matched point using the raw imagery and, only after, to apply filters to search points in areas where the previous search failed. This allows to operate at several pyramidal levels (with different resolution) independently and in different ways, e.g. making one or more filtering cycles.

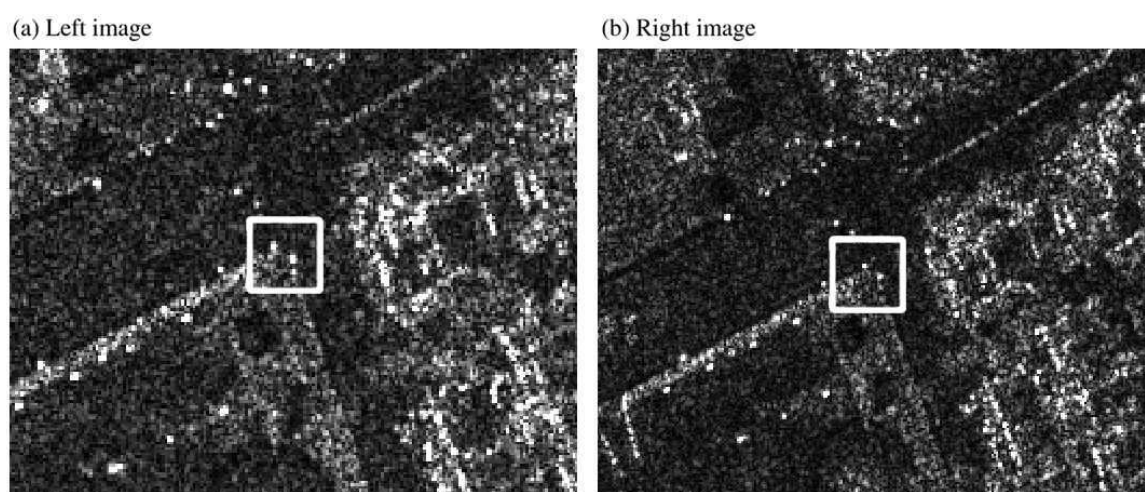


**Figure 6.** Example of homologous points in SAR imagery

### 3.1.2. Image matching strategy

The image matching strategy is based on an hierarchical solution with a geometrical constrain, and the corresponding points (actually, so-called primitives) are searched using an area based matching criterion and analysing the signal-to-noise ratio (SNR) [17]. In this sense, the peculiarity of the proposed algorithm is to use the image orientation model to limit the search area of the corresponding primitives, allowing a fast and robust matching. Primitives are searched directly in the object space re-projecting and re-sampling the stereo images on a regular grid in the ground reference system. Starting from a ground point with a selected height, the orientation model provides point image coordinates. It is thus possible to back-transfer the SAR radiometric information from slant-range to ground geometry.

From the practical point of view, after images preprocessing and area selection, a 3D grid is generated in ground geometry, with several layers slicing the entire height range. Starting from this 3D grid, by means of the orientation model, the two images are re-projected on each layer creating two voxel sets (one for left and one for right image). Through this process (Figure 7), the two generated voxel sets contain the geometrically corrected radiometric information in the same ground reference system.

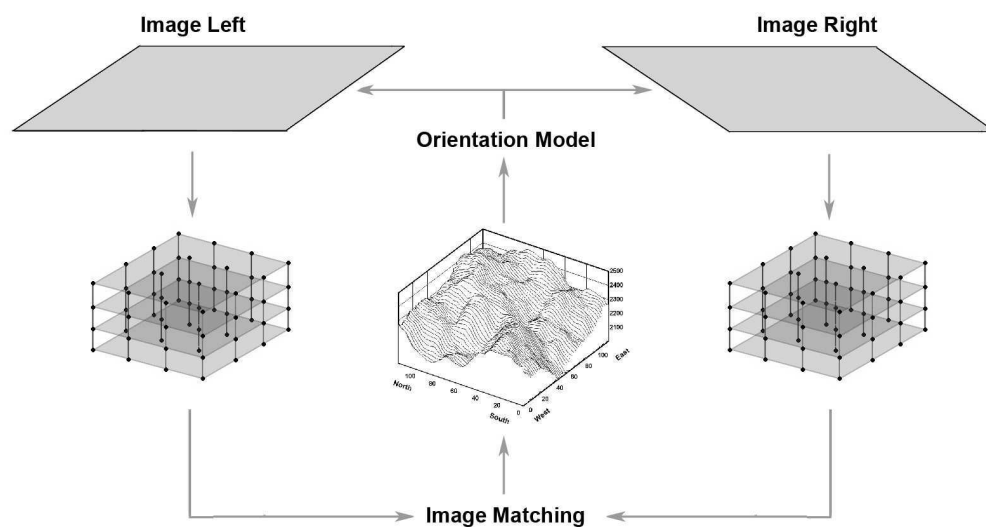


**Figure 7.** Geometrical constrain and voxel generation

At this point, for each horizontal position (X,Y) of the 3D grid, the main objective is to identify the correct height comparing the two voxel sets. This correct height corresponds to the best matching of the two voxels (for left and right image) at the same height; therefore, to this aim, the search can be conveniently carried out along vertical paths. During the algorithm development, different primitive models have been considered (i.e. Area Based Matching or Feature Based Matching [21, 22]), and the experimental results have highlighted that a normalized cross-correlation (NCC) linked with a signal-to-noise ratio analysis is the more efficient and accurate method. Overall, for each horizontal position (X,Y), the search of the corresponding primitives consists of the following steps:

- compute the NCC values along the vertical search path
- find out the maximum NCC value along the vertical search path (Figure 8)

- analyse the NCC profile and compute the vertical SNR according to the formula (10):

$$SNR_v = \frac{1 + \rho_{max}}{1 + \bar{\rho}} \quad (10)$$

where  $\rho_{max}$  and  $\bar{\rho}$  are respectively the maximum and mean value of NCC along the vertical search path; note that this search mainly examines the correspondence of primitives in West-East direction for each horizontal layer, that is orthogonally to the direction of the orbits of the considered SAR satellite

- to strength the matching, a second search is performed moving the correlation windows in North-South direction in the selected horizontal layer (Figure 8), starting from the height corresponding to the found NCC maximum value; accordingly to the same formulation (10) a second value  $SNR_p$  is computed
- if  $\rho_{max}$  and both  $SNR_v$  and  $SNR_p$  are higher than the respectively chosen thresholds, the primitives are considered matched and the height value for the horizontal position (X,Y) is finally determined

At the end of this process, after investigating and finding all the corresponding primitives for each (X,Y) position, an irregular DSM (point cloud) in (X,Y,Z) coordinates is obtained.

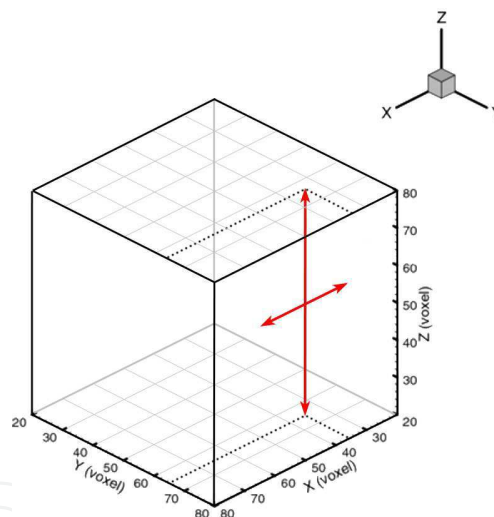


Figure 8. Search paths

### 3.1.3. Pyramidal approach

The described matching strategy is used in a coarse-to-fine hierarchical solution, following a standard pyramidal scheme based on a multi-resolution imagery approach. The advantage of this technique is that, at lower resolution, it is possible to detect larger structures whereas, at higher resolutions, small details are progressively added to the already obtained coarser DSM. The procedure starts choosing a suitable image multi-looking considering the original image resolution.

In this way, at each pyramid step, an intermediate DSM is extracted and it is modeled by the triangular irregular network (TIN) using a 2D Delauney triangulation method. Further,

DSM is interpolated on a regular grid in the ground reference system, becoming the input for the next pyramid level. Correspondingly, for each horizontal position (X,Y), the height coming from the DSM obtained in the previous pyramid step is selected as starting point for the vertical search path, whereas at the first iteration just a plane with a mean elevation is set as reference DSM. In this respect, it is worth to underline that, differently from other approaches [1], no external DSMs (for example SRTM DEM or ASTER DEM) are needed to guide matching.

As long as the resolution and pyramid level increase, and the DSM approaches the final solution, the mentioned discretization of the entire height range is correspondingly refined, so that the height step between the layers of the 3D grid, and also the number of the considered layers, decreases (Figure 9).

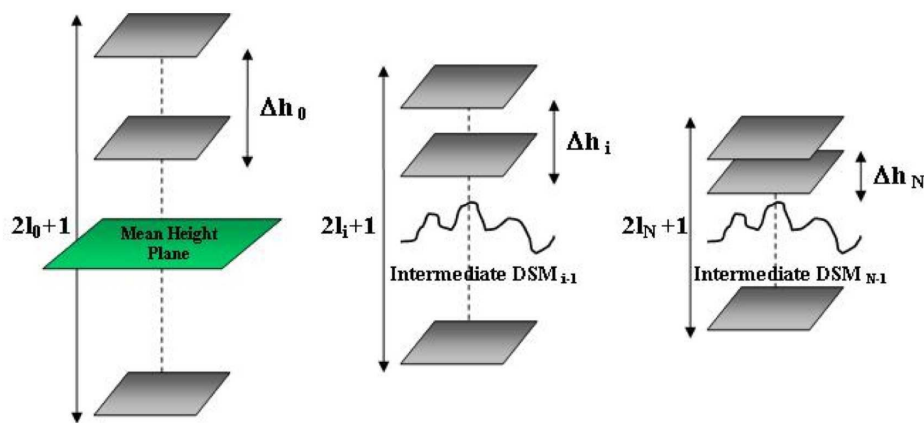


**Figure 9.** Coarse-to-Fine approach

Finally, in the algorithm flowchart (Figure 10), the complete radargrammetric approach is summarized and schematically illustrated.

#### 4. Applications

Several tests were carried out to evaluate the effectiveness of the proposed radargrammetric tool. At first, the accuracy of the radargrammetric rigorous model and RPCs model were evaluated. Then, the accuracy of the extracted DSMs was computed comparing the DSMs extracted with a more accurate reference DSM (ground truth) obtained with the airborne LiDAR technology, to assess the potential and the reliability of the overall radargrammetric DSMs generation strategy. Three test sites, Merano, Trento, Como (Northern Italy) have been selected considering their main features, and different analyses were developed as outlined hereafter:

- Merano test site: analysis of foreshortening and layover effect on DSM accuracy and comparison between Spotlight imagery;
- Trento and Como test sites: analysis of radargrammetric potentiality over forested areas and study of advantages using ascending and descending stereo pairs.

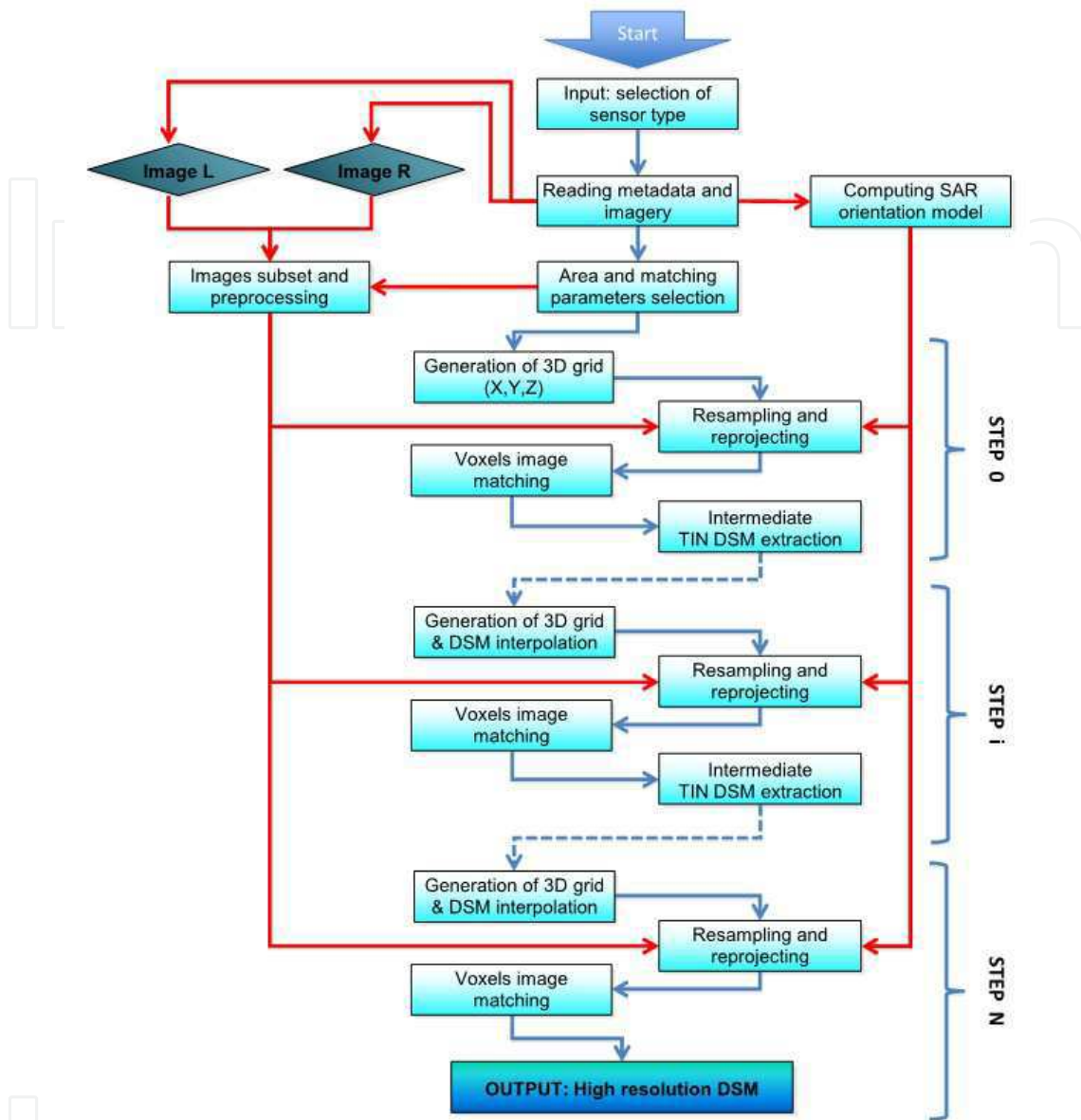


Figure 10. Radargrammetric workflow

#### 4.1. Orientation and DSM assessment strategy

As regards orientation, both the rigorous radargrammetric and the RPFs model with RPCs obtained through the implemented generation tool were considered. The accuracy was evaluated as RMSE of the residual between estimated and known coordinates of the Check Points (CPs).

The RPCs were generated on the basis of the rigorous orientation model, without the use of GCPs. In all these cases, the RPCs generation tool estimated about 20 coefficients only, instead of the 78 coefficients generally employed in the third order RPFs, avoiding the overparametrization, and selecting only the estimable and significant parameters as mentioned before.

A homogeneous DSM assessment procedure has been considered in the different tests. It is based on a comparison with a reference (ground truth minus assessed DSM) using the scientific software DEMANAL (developed by K. Jacobsen - Leibniz University of Hannover, Germany) and the accuracy statistics are computed at the 95% probability level.

#### 4.2. Merano test site

Merano is situated in the Autonomous Province of Bolzano, in Trentino Alto Adige Italian region. The area is characterized by a great cultivated plain area (the Adige river valley), where the city of Merano is located, at a mean altitude of 300 m, surrounded by mountains up to 2000 m. The available data for the experiment is a COSMO-SkyMed Spotlight stereo-pair; the imagery belongs to the Level 1A (SCS) category products, that is focused data in complex format, in slant range and zero-Doppler projection. The imagery main features are listed in Table 2.

Area	Acquisition date	Coverage [ $km^2$ ]	Incidence Angle [deg]	Orbit	B/H
Merano	30/11/2009	10 x 10	25.90	Desc	0.60
	02/11/2009	10 x 10	42.30	Desc	

**Table 2.** CSK Merano: features of test site imagery

As concerned the ground truth, a LiDAR DTM (mean elevation accuracy of 0.25 m and horizontal posting 2.50 m), has been used as reference for the DSMs assessment. These data are available on the Provincia Autonoma di Bolzano website. Unfortunately, it has not been possible to get a DSM, and not a DTM (vegetation and buildings filtered out), for performing the comparison. Two different tiles with extension of 2-3  $Km^2$  were considered, which were selected to test the potentialities of the radargrammetric approach with different morphologies and in some difficult cases, where SAR imagery distortions (i.e. foreshortening, layover) inherit the image matching.

Twenty Ground Control Points were used to evaluated the stereo pair orientation. The horizontal coordinates of which were derived from cartography (scale 1:5000), whereas the heights come from the LiDAR DTM.

BIAS CPs			ST. DEV. CPs			RMSE CPs		
East	North	Up	East	North	Up	East	North	Up
0.69	-1.96	-0.15	3.43	2.31	1.94	3.50	3.03	1.95

**Table 3.** CSK Merano: radargrammetric model accuracy [m]

The horizontal accuracy is at level of 3.0 - 4.0 m, and the vertical one is around 2.0 m (Table 3).

BIAS CPs			ST. DEV. CPs			RMSE CPs		
East	North	Up	East	North	Up	East	North	Up
0.03	-1.64	1.35	3.42	2.31	2.22	3.42	2.84	2.60

**Table 4.** CSK Merano: RPFs model accuracy [m]

The generated RPCs were used to orientate the stereo pairs. The accuracy level was close to the one achieved by the rigorous orientation model. Proving the effectiveness of the RPCs generation tool implemented in SISAR (Table 4).

Starting from the point clouds, two DSMs were generated and assessed on a 2 m posting. As regards the DSMs accuracy, results of Tile 1 (Figure 11 (a)) highlight that over a flat area the RMSE is better than 3 m (Table 5). Thanks to a quite dense point cloud generated even over forested areas, the DSM standard deviation raises to 4 m. A large negative bias is present, due to the forest (mean height canopy about 15 m); on the contrary, the details of urban areas were not correctly reconstructed (Figure 11 (b)).

Tile 1				
Land Cover	BIAS	ST.DEV.	RMSE	LE95
Flat	-2.03	1.94	2.80	4.54
Forested	-14.40	4.28	15.02	9.89
Tile 2				
Land Cover	BIAS	ST.DEV.	RMSE	LE95
Urban 1	-4.34	3.59	5.63	8.63
Urban 2	-4.92	3.40	5.98	9.11

**Table 5.** CSK Merano: DSMs accuracy [m]

In this case, it should be taken into account that the generated DSMs were compared with the reference DTM, which does not include vegetation and buildings. This is the reason of a part of the differences between the compared surfaces and this turns of particular interest over forested areas, where the radargrammetric approach was able to generate a dense points cloud despite the quite low coherence between images, in comparison to the InSAR technique. In these areas the differences are mainly due to the forest and the bias values are representative of the canopy height (apart from the already known effect of radar penetration into the canopy, causing a height underestimation around 25-30%) [23].

The urban area represented in Tile 2 (Figure 12 (a)) has been chosen because it also contains some of the most common geometric distortions that characterize SAR imagery. The relief is affected by foreshortening and layover. Foreshortening compresses features which are tilted toward the radar. Two urban areas not affected by distortions have been selected to evaluate the accuracy of the extracted DSM. The accuracy was about 6 m for both areas. In these cases, unlike the forest canopy in Tile 1, the buildings are not correctly reconstructed. The bias is only 5 m and it is not representative of the average building heights.

To see the effect of radar distortions, an image of Tile 2 has been orthorectified using the extracted DSM. During orthorectification process, layover and foreshortening situations are stretched back to their correct positions and pixels are stretched or smeared, creating areas where the matching algorithm cannot find homologous points due to lack of radiometric information. These areas are easily recognizable in the error map (Figure 12 (b) below, red zone) because they are characterized by the highest values of height discrepancies (about 30 m) between the extracted DSM and the reference.

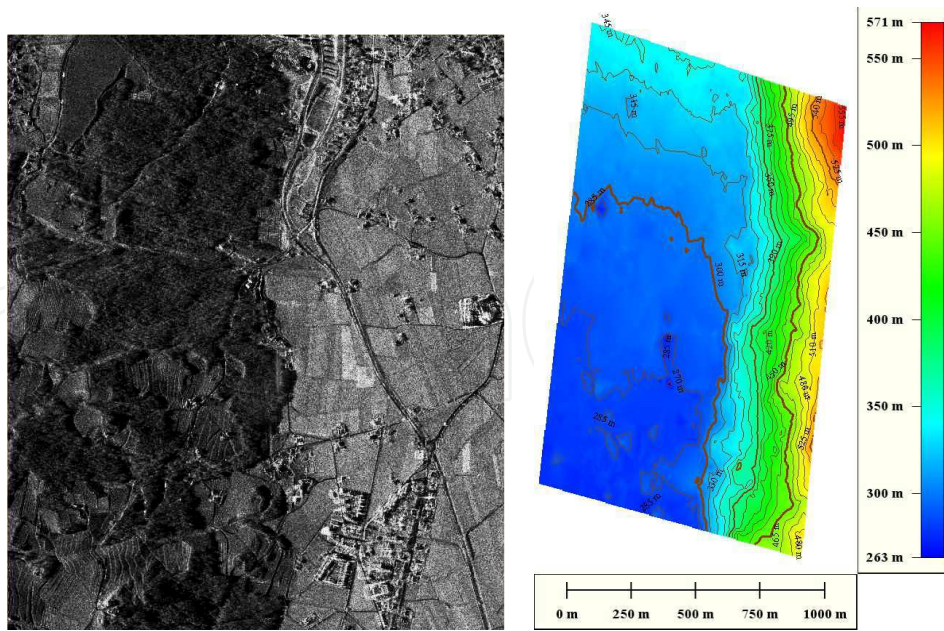


**Figure 11.** CSK Merano Tile 01: image screenshot (a) and extracted DSM (b)

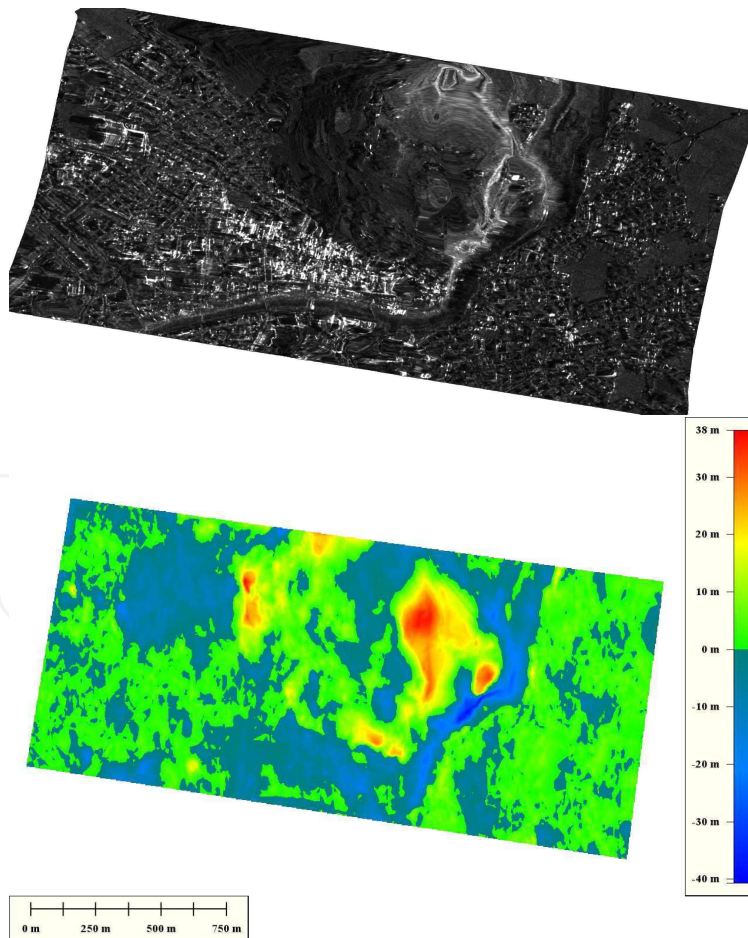


**Figure 12.** CSK Merano Tile 02: orthorectified image (a) and error map (b)

### 4.3. Trento test site

Trento city area is characterized by a dense urban morphology located inside typical hills of mountainous alpine territory.

Twelve TerraSAR-X SpotLight images have been acquired, six in descending and six in ascending mode (Table 6). A LiDAR airborne DSM supplied for free by the Provincia Autonoma di Trento was available as reference.

Area	Acquisition date	Coverage $km^2$	Incidence Angle (deg)	Orbit	B/H
Trento	<b>19/01/2011</b>	5 x 10	24.10	Desc	0.35
	01/01/2012	5 x 10	24.13	Desc	
	27/03/2013	5 x 10	24.15	Desc	
	<b>14/01/2011</b>	5 x 10	38.95	Desc	
	07/01/2012	5 x 10	38.89	Desc	
	10/03/2013	5 x 10	38.91	Desc	
	<b>22/01/2011</b>	5 x 10	31.10	Asc	0.35
	09/01/2012	5 x 10	31.14	Asc	
	04/04/2013	5 x 10	31.15	Asc	
	<b>16/01/2011</b>	5 x 10	44.19	Asc	
	31/03/2012	5 x 10	44.22	Asc	
	24/02/2013	5 x 10	44.19	Asc	

**Table 6.** TSX Trento: features of SpotLight imagery

13 GPs were used to evaluate the orientation accuracy coming from GPS survey. The accuracy is similar to COSMO-SkyMed, around 3 m (Table 7).

BIAS CPs			ST. DEV. CPs			RMSE CPs		
East	North	Up	East	North	Up	East	North	Up
-1.17	-1.07	0.06	5.78	3.12	3.24	5.89	3.29	3.24

**Table 7.** TSX Trento: radargrammetric model accuracy [m]

The generated RPCs were used to orientate the stereo pairs and the results of RPCs applications are presented in Table 8 for TerraSAR-X data. The accuracy level is close to the one achieved by the rigorous orientation model, showing the effectiveness of the RPCs generation tool implemented in SISAR.

As regards the pre-processing step for the DSM extraction, a multi-temporal filter has been used to reduce speckle and enhance images features. The three images with the same incidence angle have been co-registered (stack generation).

BIAS CPs			ST. DEV. CPs			RMSE CPs		
East	North	Up	East	North	Up	East	North	Up
-1.35	-0.93	0.90	6.13	3.23	3.55	6.28	3.36	3.66

**Table 8.** TSX Trento: RPFs model accuracy [m]

In Table 6, the master images of each stack are highlighted in bold. Multi-temporal averaging filtering technique has been performed using a kernel (11x11 pixels) available in the ESA Next SAR toolbox v. 5.05. Starting from twelve speckled images, two same-side filtered stereo-pairs (one ascending, one descending) were formed and used for the DSMs generation after separate processing.

The two stereo pairs were processed separately and the corresponding point clouds were assessed. The height differences were computed by interpolating with a bilinear method the analysed DSM over the reference LiDAR DSM. A tile featured by a mixed morphology was selected for the analysis. The results of the accuracy assessment are presented in Table 9. The point clouds derived from the ascending and descending stereo pairs, directly produced by matching procedure without any further post-processing, have been analyzed.

<b>Point cloud assessment</b>			
<b>Ascending</b>			
BIAS	ST.DEV.	RMSE	Points
1.90	6.59	6.86	603420
<b>Descending</b>			
BIAS	ST.DEV.	RMSE	Points
0.60	6.79	6.82	702990
<b>SRTM filtered point cloud assessment</b>			
<b>Ascending (about 6 % points removed)</b>			
BIAS	ST.DEV.	RMSE	Points
1.86	6.36	6.63	563598
<b>Descending (about 7 % points removed)</b>			
BIAS	ST.DEV.	RMSE	Points
0.61	6.29	6.32	650019

**Table 9.** TSX Trento: point cloud assessment results [m]

The accuracy was around 7 m. Some outliers were detected in the point clouds, probably due to mismatching, causing incorrect morphological reconstruction in small areas.

<b>Ascending</b>				
Filter	BIAS	ST.DEV.	RMSE	Points
No	1.54	6.55	6.73	259351
Yes	1.57	6.43	6.62	252628
<b>Descending</b>				
Filter	BIAS	ST.DEV.	RMSE	Points
No	0.27	7.93	7.93	268552
Yes	0.33	6.67	6.68	254468
<b>Final DSM</b>				
	BIAS	ST.DEV.	RMSE	Points
	1.05	6.37	6.45	275827

**Table 10.** TSX Trento: DSMs assessment results (4x4 meters posting) [m]

To remove these outliers, a free available low resolution DSM (SRTM DEM, 3' grid posting) was used as reference. The point clouds were compared with SRTM, and the height

differences computed. When the difference was greater than a fixed threshold (25 meters), the corresponding point was rejected. As shown in Table 9, no significant improvement in term of RMSE were detected; on the other hand, about 6-7% of points were removed. Three DSMs were generated and assessed on a 4 m posting. In Table 10, the results of the interpolated DSMs are shown. The ascending and descending DSMs were generated using the points clouds (both filtered and no filtered). A merged DSM was generated using a combination of the filtered point clouds to achieve the best result. The accuracy was around 7 m and 8 m for the ascending and the descending no filtered DSMs respectively. An improvement of 1 m in term of RMSE only for the descending filtered DSM was detected. Overall, the merging slightly improved the results in term of RMSE (about 0.5 meters), though more details were observed through a visual inspection.

#### 4.4. Como test site

Como city area is characterized by a dense urban morphology.

Area	Acquisition date	Coverage $km^2$	Incidence Angle (deg)	Orbit	B/H
Como	07/08/2011	10 x 10	28.90	Asc	0.60
	17/06/2011	10 x 10	50.80	Asc	
	24/06/2011	10 x 10	27.80	Desc	0.80
	28/06/2011	10 x 10	55.40	Desc	

**Table 11.** CSK Como: features of SpotLight test site imagery

Imagery suitable for radargrammetric application, were acquired on Como test fields. Two same-side stereo pair were available, acquired on ascending and descending orbits respectively. Images features are listed in Table 11.

As a ground truth, a LiDAR DSM provided by the "Regione Lombardia" was used. The reference DSM has an horizontal spacing of 1 m and its vertical accuracy is about 0.25 m.

Considering that a descending and an ascending stereo pairs were available, the DSM could be reconstructed using two different points of acquisition. Starting from the ascending and descending points clouds, three DSMs were generated and assessed, estimating the heights on a 5 m x 5 m grid by a linear interpolation, after a Delaunay triangulation. The merged DSM was generated using a combination of the point clouds that were previously filtered, removing the matched points with lower correlation. Table 12 shows the assessment results. The accuracy ranges from 8 to 10 meters, for the ascending and the descending DSMs, and decrease to 7 m in the merged product. This test highlights that, the use of at least two stereo pairs acquired under different look side seems to be an effective strategy to overcome the limitations arising from SAR imaging system such as, layover, foreshortening and shadow.

## 5. Conclusions and future prospects

### 5.1. Conclusions

This chapter discussed on high resolution satellite SAR imagery for DSMs generation with a radargrammetric stereo-mapping approach. The main features of the radargrammetric

Total				
DSM	BIAS	ST.DEV.	RMSE	LE95
Ascending	-1.07	7.79	7.86	21.87
Descending	1.53	10.24	10.35	33.14
Merged	-1.10	6.94	7.02	18.14
Wooded				
DSM	BIAS	ST.DEV.	RMSE	LE95
Ascending	-0.69	7.10	7.14	18.10
Descending	1.32	8.53	8.63	27.06
Merged	-0.88	6.07	6.14	15.55
Urban				
DSM	BIAS	ST.DEV.	RMSE	LE95
Ascending	-1.45	8.32	8.45	22.01
Descending	1.73	11.86	11.98	38.10
Merged	-1.40	7.59	7.72	20.18

**Table 12.** CSK Como: DSM Absolute Error [m]

procedure implemented in SISAR package were defined. It outlined the orientation model and it focused on the original matching strategy, presently patent pending by the University of Rome "La Sapienza". It is established on area based primitive model and on an hierarchical solution with geometrical constrain. The leading idea was to search the corresponding primitives directly in the object space, re-projecting and re-sampling the stereo images into a 3D ground grid. The correspondences are looked analysing the signal-to-noise ratio (SNR) along two perpendicular search paths. A specific speckle dynamic filtering technique was designed and embedded into the radargrammetric procedure, based on three standard speckle filters (Lee, Kuan, GammaMap).

The complete radargrammetric processing chain was developed and implemented using the IDL development environment. To demonstrate its mapping capabilities, several tests were carried out using high resolution SAR satellite imagery acquired in Spotlight mode and coming from different platforms (COSMO-SkyMed, TerraSAR-X). A homogeneous DSM assessment procedure was considered in different tests, based on the comparison with a reference ground truth using the scientific software DEMANAL. Summarizing the main results of other tests, the DSMs vertical accuracy was strictly related to the terrain morphology and land cover. In case of limited SAR distortions (layover and foreshortening) the observed RMSE values ranged from 3-4 meters over bare soil and forest to 6-7 meters in more complex urban areas. Regarding the area of Como, the accuracy became worse. The terrain morphology might be conveniently reconstructed using at least two same-side stereo pairs in ascending and descending modes.

Finally, radargrammetric stereo-mapping approach appears a valuable tool to supply topographic information. It is likely to become an effective complement/alternative to InSAR technique, since it may work using a couple of images with a good performance even over areas (forested or vegetated areas) characterized by low coherence values.

## 5.2. Some suggestions for the future

Although the experimental results have demonstrated that StereoSAR approach has the capability to give good and encouraging results, there are still a lot of challenging issues which need to be considered for further improvements. Hereafter are listed some ideas for the future:

- orientation model customization and possible refinement: additional tests should be performed on data acquired by the expected Sentinel-1 SAR satellite sensor;
- self-tuning matching parameters: the automatic determination of the matching parameters is necessary to improve success rate and decrease mismatches. These parameters: size of the correlation window and search distance and the threshold values, should be evaluated in analysing the radiometric information of the higher-level image pyramid matching and in using them at the current pyramid level;
- efficient quality control measures: a quality control procedure of matched points should be developed by well-defined precision measures that are derived from the primitive model and from the parameter estimation;
- efficiency improvement in urban areas: to model the complicated urban morphology, specific algorithms must be developed, accounting for remarkable features as double bounces or building shadows. Some preliminary investigations applying semiglobal matching [24] to quasi-epipolar image previously generated gave promising results;
- algorithm optimization: a speed-up of the matching process could be achieved exploiting the high computational performance of Graphic Processing Units (GPUs). Reliability and accuracy could be improved, allowing concurrent processing of multiple stereo-pairs (i.e. ascending and descending ones);
- accounting for polarimetric information: studying algorithms and techniques for optimizing DSMs generation from full SAR polarimetric data [25] through radargrammetry. In particular, the potential of polarimetric imagery and their derived products (i.e. span, entropy, H-A- $\alpha$  classification maps) should be investigated to enhance the image matching;
- interferometry and radargrammetry tight integration: the two techniques should be considered to exploit the 3D mapping potential of high resolution satellite SAR data: radargrammetric DSMs can be used within the InSAR processing chain to simplify the unwrapping process to avoid areas affected by phase jumps.

## 6. Acknowledgements

The Authors are indebted with:

- Prof. K. Jacobsen for the DEMANAL software
- Dr. R. Lanari, PI of the Italian Space Agency Announcement of Opportunity for COSMO-SkyMed project "*Exploitation and Validation of COSMO- SKyMed Interferometric SAR data for Digital Terrain Modelling and Surface Deformation Analysis in Extensive Urban Areas*", within which the Como imagery were made available
- Regione Lombardia, for making available the LiDAR DSM
- Prof. Uwe Soergel, PI of the international DLR project "*Evaluation of DEM derived from TerraSAR-X data*" organized by the ISPRS (International Society for Photogrammetry and Remote Sensing) Working Group VII/2 "SAR Interferometry", within which the TerraSAR-X imagery were made available

## Author details

Paola Capaldo\*, Francesca Fratarcangeli, Andrea Nascetti, Francesca Pieralice, Martina Porfiri and Mattia Crespi

Geodesy and Geomatic Division - DICEA, University of Rome "La Sapienza", Italy

\*Address all correspondence to: [paola.capaldo@uniroma1.it](mailto:paola.capaldo@uniroma1.it)

## References

- [1] H. Raggam, K. Gutjahr, R. Perko, and M. Schardt. Assessment of the Stereo-Radargrammetric Mapping Potential of TerraSAR-X Multibeam Spotlight Data. *IEEE Transactions on Geoscience and Remote Sensing*, 48(2), 2010.
- [2] T. Toutin. Stereo RADARSAT for Mapping Applications. *2nd International ADRO Symposium, Montreal, Canada, 1998*.
- [3] P. Capaldo, M. Crespi, F. Fratarcangeli, A. Nascetti, and F. Pieralice. High resolution SAR imagery. Radargrammetric application with COSMO-SkyMed. *IEEE Geoscience and Remote Sensing Letters*, 8.
- [4] Franz W. Leberl. *Radargrammetric image processing*. Norwood, MA : Artech House, 1990.
- [5] S. Meric, F. Fayard, and E. Pottier. Radargrammetric SAR image processing. In: *Pei-Gee Peter Ho (Eds.), Geoscience and Remote Sensing, Intech*, pages 421–454, 2009.
- [6] T. Toutin and L. Gray. State-of-the-art of elevation extraction from satellite SAR data. *ISPRS Journal of Photogrammetry & Remote Sensing*, 55:13–33, 2000.
- [7] G. La Prade. An Analytical and Experimental Study of Stereo for Radar. *Photogrammetric Engineering*, 29(2):294–300, 1963.
- [8] T. Toutin. Geometric processing of remote sensing images: models, algorithms and methods (review paper). *International Journal of Remote Sensing*, 10:1893–1924, 2004.
- [9] P. Capaldo, M. Crespi, F. Fratarcangeli, A. Nascetti, and F. Pieralice. A radargrammetric orientation model and a RPCs generation tool for COSMO-SkyMed and TerraSAR-X high resolution SAR. *Italian Journal of Remote Sensing / Rivista Italiana di Telerilevamento*, 44(1):55–67, 2012.
- [10] P. Capaldo. High resolution radargrammetry with COSMO-SkyMed, TerraSAR-X and RADARSAT-2 imagery: development and implementation of an image orientation model for Digital Surface Model generation, 2013. PhD Thesis - Supervisor: Crespi M.
- [11] P. Capaldo, M. Crespi, F. Fratarcangeli, A. Nascetti, F. Pieralice, M. Porfiri, and T. Toutin. DSMs generation from COSMO-SkyMed, RADARSAT-2 and TerraSAR-X imagery on Beauport (Canada) test site: evaluation and comparison of different radargrammetric approaches. *ISPRS Hannover Workshop 2013*, 2013.

- [12] C.V. Tao and Y. Hu. The rational function model. A tool for processing high resolution imagery. *Earth Observation Magazine*, 10(1):13–16, 2001.
- [13] H.B. Hanley and C. S. Fraser. Sensor orientation for high-resolution satellite imagery: further insights into bias-compensated RPC. *Proceeding of XX ISPRS Congress, Istanbul, Turkey*, 2004.
- [14] F. Sansò, A. Dermanis, and A. Gruen. An overview of data analysis methods in geomatics. . *Geomatic methods for the analysis of data in the earth sciences*, Springer, 2000.
- [15] M.A. Box, M. Jenkins, F. Reinsel, and F. Time Series Analysis-Forecasting and Control. *Prentice Hall*.
- [16] G. Strang and K. Borre. *Linear Algebra, Geodesy and GPS*. 1997.
- [17] Yi Ma, Stefano Soatto, Jana Kosecka, and S. Shankar Sastry. *An invitation to 3D Vision: from images to geometric models*, volume 1 of 1. Springer, 2004.
- [18] Christian Heipke. Overview of image matching techniques. *OEEPE workshop on Application of digital photogrammetric workstations*, 1996.
- [19] T. Heuchel. Experience in applying matching techniques using images from digital cameras. *Photogrammetric Week Wichmann, Verlag*, 05:181–188, 2005.
- [20] A. Nascetti. High resolution radargrammetry: development and implementation of an innovative image matching strategy, 2013. PhD Thesis - Supervisor: Crespi M.
- [21] W. Forstner. A feature based correspondence algorithm for image matching. *ISP Comm III - Int Arch. of photogrammetry*, pages 150–166, 1986.
- [22] C. Harris and M. Stephens. A combined corner and edge detector. *Fourth Alvey Vision Conference*, pages 147–151, 1988.
- [23] R. Perko, H. Raggam, J. Deutscher, K. Gutjahr, and M. Schardt. Forest assessment using high resolution SAR data in X-Band. *Remote Sensing*, 3(4):792–815, 2011.
- [24] Hirschmuller H. Stereo Processing by Semiglobal Matching and Mutual Information. *IEEE Trans on Pattern Analysis and Machine Intelligence*, pages 328–341, 2008.
- [25] Lee J-S. Pottier E. *Polarimetric Radar Imaging: From Basics to Applications*. CRC Press, Taylor and Francis Group, 2009.